A LASER DOPPLER ANEMOMETER FOR VISCOUS SUBLAYER MEASUREMENTS

By

MICHAEL E. KARPUK

Bachelor of Science

Oklahoma State University

Stillwater, Oklahoma

1972

Submitted to the Faculty of the Graduate College
of the Oklahoma State University
in partial fulfillment of the requirements
for the Degree of
MASTER OF SCIENCE
May, 1974

OKLAHOMA
STATE UNIVERSITY
LIBRARY

SEP 3 1974

A LASER DOPPLER ANEMOMETER FOR VISCOUS

SUBLAYER MEASUREMENTS

Thesis Approved:

W. A. Tiederman
Thesis Adviser

D K McLaughlin

J A Wiebelt

N N Durham
Dean of the Graduate College

891348

ACKNOWLEDGMENTS

I would like to thank above all my thesis advisor, Dr. W. G. Tiederman for his help and criticisms during this study. I would also like to thank Dr. D. K. McLaughlin who first aroused my interest in laser Doppler anemometry.

I am also very grateful to Sandra Ramm who typed the major part of the rough draft, helped with the data runs and data reduction and drew some of the figures.

There are many people who have helped with both work and ideas. I would like to express my gratitude to Scott Quigley, Bill Adcox, Tim Troutt, and Gene Kouba. I would also like to thank Judy Lacy for typing the final copy of this thesis.

TABLE OF CONTENTS

LIST OF TABLES

LIST OF FIGURES

NOMENCLATURE

b	Diameter of the laser beam
d	Diameter of the probe volume
f_D	Doppler frequency
f_L	Focal length of the lens
f_p	Pedestal frequency
k	Constant in turbulence model related to intensity
l	Location of the center of the probe volume
N	Number of realizations in a set of data
Re	Reynolds Number
S	Fringe spacing
s	Velocity gradient in the turbulence model
t	Time
U	Streamwise velocity component
U_t	Time average streamwise velocity
U_i	Individual streamwise velocity realization
U_m	Mean streamwise velocity
U^+	Nondimensional streamwise velocity
U_τ	Shear velocity
u'	Root mean square of the streamwise velocity fluctuations
u'_c	Corrected root mean square of the streamwise velocity fluctuations
V	Velocity normal to the wall
W	Channel width

w	Probe volume width
y	Distance normal from the wall
y^+	Nondimensional normal distance from the wall
λ	Wave length of light
θ	Angle of beam intersection
υ	Kinematic viscolity
ω_i	Weighting function

CHAPTER I

INTRODUCTION

The viscous sublayer is the region in a turbulent boundary layer that adjoins the wall. Viscous forces predominate and the time average velocity profile is linear. However, the flow field is not laminar as the root-mean-square of the velocity fluctuations can be as much as .40 of the local mean. Although the physical size of the sublayer is small (less than .02 inch for the measurements presented here) there is a sharp change in velocity across the sublayer. The combination of these three features of the sublayer, high turbulence, small size, and large velocity gradient, makes laser Doppler anemometry measurements difficult. Consequently, any laser Doppler anemometer which is designed to make velocity measurements in this region must have good spatial resolution as well as the capability to measure a wide range of velocities. This thesis describes such an anemometer, outlines a correction for the biasing effects of a velocity gradient and presents the results of measurements in a two dimensional channel flow of water.

Description of a Simple Laser Doppler Anemometer

A basic dual scatter laser Doppler anemometer is shown in Figure 1. A single laser beam is split into two equally intense parallel beams. The beams are crossed with a focusing lens. At the beams intersection,

a fringe field is formed. This area is known as the probe volume. When a particle that is entrained in the flow moves through the probe volume, light is scattered. This scattered light which is modulated by the fringes is collected by a receiving lens and is detected by a photomultiplier.

The photomultiplier output for a single particle moving through the probe volume is also shown in Figure 1. There are two components in the wave form, a pedestal frequency, which is a result of the Gaussian distribution of the intensity of the laser beam and a Doppler frequency which is a result of the interference fringes. The relationship between the Doppler frequency and the particle velocity is

$$U = \left(f_D\right)\left(S\right) = \left(f_D\right)\left(\lambda\right) \; / \; 2 \sin\left(\theta/2\right) \qquad (1\text{-}1)$$

where f_D is the Doppler frequency, S is the fringe spacing, is the wave length of light used and is the angle of beam intersection.

To measure the Doppler frequency it is generally necessary to eliminate the pedestal frequency. This is usually done with an electronic high-pass filter. This filter limits the range of velocities that can be measured by the anemometer. The setting of the filter is difficult when the turbulence is high or when the velocity to be measured is not well known.

There are several methods used to measure the Doppler frequency, among them are period counters, spectrum analyzers, frequency trackers, and filter banks.

Scope of This Study

The anemometer used in this study is based on a device described earlier by Tiederman, McLaughlin and Reischman (1973). Two modifications, pedestal frequency canceling optics and a one dimensional probe volume miniaturization were made to allow viscous sub-layer measurements. These modifications as well as the data processing system and flow facility are described in the second chapter.

Mean velocity and fluctuating velocity measurements are presented for two Reynolds numbers and compared to other studies in the third chapter.

Appendix A summarizes the statistical bias correction derived by McLaughlin and Tiederman (1973). Appendix B shows the effect of a finite sized probe volume in a flow with a large velocity gradient. The data are presented in Appendix C.

CHAPTER II

EXPERIMENTAL APPARATUS AND TECHNIQUES

This chapter will describe the flow facility, laser Doppler anemometer and the data reduction techniques.

The Laser Doppler Anemometer

The anemometer is based on a device described by Tiederman, McLaughlin and Reischman (1973). The general configuration is shown in Figure 2. The anemometer's laser beams are parallel to the side walls of the channel. This allowed near wall measurements to be made without having the laser beams penetrate the wall within the view of the detecting optics, thus greatly improving the signal to noise ratio. It also allows the use of the smallest dimension of the probe volume, 90^{o} to the plane of the beams, to be normal to the wall.

Scattered light is detected at a 90^{o} angle. The scattering efficiency is lowest at this angle but this configuration allows a simple traversing mechanism to be used.

To circumvent the difficulties associated with the continuous wave mode, such as signal dropout and frequency tracking in low-velocity, high fluctuation regions, the individual realization mode was used (see Donohue, McLaughlin and Tiederman, 1972). The essential feature of the individual realization mode is that the scattering particles are

so dilute that the signal is discontinuous and individual Doppler bursts are caused by only one particle.

Probe Volume Shape and Size

In making viscous sublayer measurements a major consideration is spatial resolution or probe volume size. The size of the probe volume is determined by the diffraction limit of the lens and for beams with a Gaussian intensity distribution this limit is given by the equation

$$d = \frac{f_L \lambda}{2b} \qquad (2\text{-}1)$$

where b is the diameter of the beams and f_L is the focal length of the lens. The size of the probe volume may be reduced by expanding the beams before the final lens. If the probe volume is reduced in size and if the number of fringes in the probe volume remains constant, the fringe spacing must decrease. This means that the Doppler frequency will increase, the optimum size of scattering particle will decrease, and thus, the amount of scattered light will decrease (see Durst and Whitelaw, 1972). This leads to problems in the light detection system and in the electronics.

With the beams parallel to the walls the only critical dimension, 90^o degrees to the plane of the beams, can be reduced without affecting the fringe spacing. This amounts to making the probe volume cross section an oval instead of a circle. This is illustrated in Figure 3.

The oval probe volume shape does limit the measurement of particles of a high V/U ratio. The extent of this limitation will be discussed later.

Pedestal Canceling Optics

The high degree of turbulence in the viscous sublayer also causes problems in making velocity measurements. Figure 4 shows a histogram of pedestal and Doppler frequencies. As the turbulence increases the histograms broaden and can possibly overlap. Since pedestal frequencies are filtered electronically, some of the velocity realizations would be filtered. Even if the histograms do not overlap, an error in the filter setting can eliminate good data.

One way to overcome these problems is to increase the number of fringes in the probe volume, that is increase the f_D/f_p ratio. However, this causes the fringe spacing to be reduced resulting in smaller optium particle size, reduced amount of scattered light and higher Doppler frequencies. As with probe volume miniaturization these lead to light detection problems.

Another way to overcome the problem caused by turbulence is to optically cancel the pedestal frequencies. Such an optic system was originally described in detail by Bossel, Hiller and Meier (1972) and Goethert (1971). The concept used in the pedestal canceling optics is to establish two fringe patterns in the probe volume which are displaced in space by one-half of the fringe spacing or in phase by 180°. When signals from the two fringe patterns are simultaneously and independently detected and then subtracted from each other, the Doppler frequency is reinforced while the pedestal frequency is canceled.

The two phase shifted fringe patterns are established by crossing two orthogonally polarized laser beams. Each of the fringe patterns can be independently detected by passing the scattered light through a

polarization filter. One fringe set will appear at 45^{o} polarization with respect to a beam the other at -45^{o}.

The output from the differential amplifier has only the Doppler frequency. The high pass electronic filter is eliminated from the system. Thus, the range of the anemometer is greatly increased. This is particularly important when velocity fluctuations are high and when there is not a good estimate for the mean velocity.

Construction of Anemometer

Figure 5 shows the configuration of the transmitting and detecting optics of the anemometer. A Spectra Physics Model 120 5mw He-Ne laser was used. A polarization rotator was mounted on the front of the laser. Two parallel beams were obtained by using a rectangular beam splitter and mirror.

The natural tendency of the beam splitter to reflect one polarized component was used to equalize beam intensities. By turning the polarization rotator on the front of the laser, one of the beams will increase in intensity while the other decreases. To make this adjustment, the beams were reduced to 1% intensity and aimed directly into a photo diode. The polarization rotator was adjusted until the photo diode output was the same for each beam.

Two more polarization rotators were used in the system to provide the orthogonal polarization orientation for the pedestal canceling optics. The polarization of one beam was set at 90^{o} the other at 0^{o}. The polarization rotators were constructed from mica salvaged from a high voltage capacitor. The mica was sandwiched between two pieces of microscope slide glass to protect it from being scratched. Of the

several hundred pieces from the capacitor three were chosen for their clarity and half wave properties at 6328 $\overset{o}{A}$.

The beam expander was constructed from two cylinder lenses. It provides a beam expansion in the vertical plane of about four from .026 inch to .104 inch. This produced a probe volume .0096 inch long and .0024 inch wide at the $\frac{1}{e^2}$ points. However, the effective size of probe volume is determined by the photomultiplier and the data processing electronics and is a function of the size of the particle, its reflective index, supply voltage to the photomultiplier, location in the channel, and the trigger level of the Schmitt trigger. These effects will be discussed in detail later.

The size of the smallest turbulent eddy as estimated by the Taylor microscale was calculated to be .06 inch. This is approximately one order of magnitude larger than the size of the probe volume.

Alignment of the beam expander was a delicate operation. The beams were passed through the beam expander then through the focusing lens. Just before the beams crossed, a negative lens was put in the beams. This caused an image of the probe volume to be projected on the wall. The beam expander was adjusted to give a well defined oval.

Following the beam expander is the focusing lens. Its focal length was approximately eight inches. This focal length and the beam separation, which was .5 inch, uniquely determines the Doppler frequency to velocity conversion constant. The exact measure of this constant was made by placing the anemometer six feet away from the wall and measuring the separation of the beam on the wall. The conversion constant was 31,380 Hz/ft/sec.

The final element in the transmitting optics is the adjustable mirror. The mirror was adjusted so that the beams were parallel to the walls of the channel and also such that the angle made by the beam intersection was symmetric with a string hung from the ceiling. The second adjustment insured that the fringes in the probe volume were exactly in the vertical direction.

The receiving optics use a combination of two short focal length lenses to provide a large solid angle of light collection. A two inch beam splitter distributes scattered light to the two photomultipliers. Polarization filters with angle scales were mounted in front of both photomultipliers. No small aperature was used on the photomultipliers since the inexpensive lenses had considerable amount of aberation and would not focus to a sharp point, the photomultipliers had to be covered to prevent stray light, such as from the running lights of the electronics, from increasing the signal to noise ratio.

The entire anemometer was mounted on a 50 inch long one inch thick piece of aluminium. This piece was mounted on a movable traverse mechanism. To change measurement locations in the flow, the entire anemometer was moved. The accuracy of the traverse was $\pm$ .0005 inch with respect to any other point.

The location of the probe volume with respect to the wall was much harder to determine. After trying several different techniques, one was found that was the most repeatable. The technique was to find the location closest to the wall where realizations could be detected by the photomultipliers. The probe volume was moved into the wall then slowly moved out until Doppler bursts could be seen on the oscilloscope. This was done several times and found to be repeatable within a .002 inch,

or approximately one probe volume dimension. The exact location was determined after the data was reduced by the zero intercept of the velocity profile.

Data Acquisition Electonics

A block diagram of the electronic processing of the signal is shown in Figure 6. Two RCA photomultiplier tubes, a 7265 and 7326, both with a S-20 spectral response were used. They were powered by a common high voltage supply and their outputs were balanced by using different loading resistors. The differential amplifier was the pre-amplifier of a Tektronics 502A oscilloscope with a restored horizontal output. The "A-B" signal was recorded on a Sanborn Model 2000 magnetic tape recorder at 60 inches per second.

The data was replayed at 7½ inches per second into a Schmitt trigger which converts each Doppler burst into a pulse train. The pulse train is connected to both a Tektronics 564B oscilloscope and a General Radio 1192 B counter operating in the period times ten mode. The second digit of the counter output triggers the oscilloscope so that it is possible to display the pulse train whose average period is displayed on the counter. Each counter output is visually verified on the oscilloscope to make sure there are no missing pulses before the count is accepted. The verified counts are then punched on computer cards so that the mean and standard deviation of each ensemble can be calculated. Figure 7 shows two examples of the Doppler bursts and their respective pulse trains from the Schmitt trigger. The top example has no dropped pulses in the ten cycles counted by the counter and therefore the count would be accepted. The lower picture has missing

pulses in the Schmitt trigger output and consequently this count would be rejected.

Flow Channel and Seeding

The measurements were made in the two dimensional water channel facility described by Reischman (1973). The channel is 72 inches long, 12 inches high and approximately one inch wide at the mid-plane. The vertical walls are each bowed inward .060 inch along the entire length of the channel. Measurements were made 55 channel widths downstream of the sharp-edged Borda type entrance. The water is continuously recirculated with a 200 GPM pump.

An overall view of the flow facility and anemometer is shown in Figure 8.

Corrections to the Data

Two corrections were applied to the data. The first corrects the statistical biasing caused by the turbulence. The second corrects for the effect of a finite sized probe volume on the fluctuating intensity.

McLaughlin and Tiederman (1973) describe the statistical biasing present in individual realization laser Doppler anemometer measurements of turbulence. The concept is that the probability of a realization is proportional to the volume of fluid being swept through the probe volume. This causes more realizations at the high velocities than the low. The ensemble average of the velocity realizations is biased high. The correction for this effect is summarized in Appendix A and was applied to all of the data.

In the very near wall region the size of the probe volume causes errors in the fluctuating intensity measurements. The measured fluctuations are caused by not only the turbulence but also the change in mean velocity and fluctuating velocity across the probe volume. This effect is important when the change in mean velocity across the probe volume is near the average velocity through the probe volume. This effect and a correction for it are summarized in Appendix B.

CHAPTER III

EXPERIMENTAL RESULTS

The anemometer was successfully used to make measurements of the mean and root mean square of the streamwise velocity component at Reynolds numbers of 7,470 and 12,790 in the fully developed flow of water in a two dimensional channel. Here the Reynolds number is based on the mass average velocity and the channel width of one inch.

The pedestal canceling optics effectively eliminated pedestal frequency from the Doppler burst. The probe volume miniaturization increased the spatial resolution of the anemometer without biasing the measurements.

Evaluation of Pedestal Canceling Optics

In general the pedestal canceling optical system yielded high signal to noise ratios and "A-B" bursts which were relatively symmetric about zero. A small percentage of the signals were always asymmetrical. It is believed that this occurred because the scattering particles were not spherical and hence there was a tendency to scatter one polarization more effectively than the other. In any case, this was not a large effect when the system was well aligned and the pedestal canceling technique was considered to be a success.

A more quantitative estimate of the merits of the optical system can be gained by inspecting a typical histogram of the velocity

realizations in the low-velocity, high-fluctuation region. Figure 9 is such a histogram. This data was acquired at a y^+ of 7.5 and a Reynolds number of 12,790. The realizations ranged from a high of 1.39 ft/sec to a low of .08 ft/sec. $\overline{U}$ was .621 ft/sec and u' was a .230 ft/sec. The obvious point is that the system responded to an extremely broad range of velocity.

Evaluation of Probe Volume Miniaturization

The oval shape of the probe volume introduces the possibility that in regions where the ratio of V/U is large that particles could travel through the probe volume at such an angle that ten fringes would not be crossed. This possibility is obviously nil at the center of the channel but it is not apparent what will occur in the near-wall region. Using an automatic signal processor Salsman, Adcox, McLaughlin (1974) evaluated this effect upon these data by comparing the number of Doppler bursts with 13 or more consecutive cycles to the total number of bursts with two or more cycles. This ratio was constant across the flow field and thus it was concluded that the probe volume parameters had no statistically significant effect on the measurements.

The maximum size of the probe volume can be estimated from the number of fringes seen in a Doppler burst. For a typical signal to noise ratio, photomultiplier gain and Schmitt trigger setting, fringes in a Doppler burst were counted. Approximately 7% of the bursts had more fringes than the $1/e^2$ contour would indicate. It was concluded that the $1/e^2$ contour was a good estimate of the probe volume size.

Flow Measurement

Figure 10 shows the dimensional, mean velocity profile in the viscous sublayer for a Reynolds number of 7470. Both the biased, $\overline{U}_e$ estimates of the mean as well as the corrected, $\overline{U}$, estimates are shown to illustrate the magnitude of the biasing error. In this region the biased estimates are approximately 10% high. The error decreases only when the ratio of $u'/\overline{U}$ decreases. As would be expected from the law of the wall, the data is very linear. A least squares regression was used to determine the slope and the zero-velocity intercept of a straight line passing through the four points. The zero-velocity intercept of this line is believed to be the best estimate of the wall location because the accuracy of locating one point related to another is much better than locating the wall. In all of the following figures the y locations are shifted so that $y = 0$ corresponds to the zero-velocity intercept.

Figure 11 shows the normalized velocity profiles. The profiles were graphically integrated to obtain the mass-average velocity which with the channel diameter was used to calculate Reynolds number. The data are in good agreement with the measurements of Patel and Head (1969). The average velocity was .855 of the maximum for the 7,470 Reynolds number and .867 for the 12,790 Reynolds number.

The shear velocity which was calculated from the slope of the velocity profiles in the viscous sublayer was used to scale the data in law of the wall coordinates

$$U^+ = \frac{U}{U_\tau} \qquad y^+ = \frac{yU_\tau}{\upsilon} \qquad (3\text{-}1)$$

Figure 12 shows the results for the near wall region. Note that the data are linear for y^+ less than 5.5. There are four data points in the viscous sublayer of the 7,740 run and three in the run at a Reynolds number of 12,790. The entire flow field is shown in Figure 13. The profile is also logarithmic in the core region. The data for $y^+ > 30$ and a least squares regression analysis were used to determine the constants in the equation

$$U^+ = A \log y^+ + B \qquad (3\text{-}2)$$

The results are summarized in Table I. The data is in fairly good agreement with Eckelmann and Reichardt (1971) and Patel and Head (1969). The 95% confidence intervals were calculated for the estimates of A & B and were found to be quite large. This large uncertainty is due to the small number of points, 4 or 5, and their closeness to each other rather than their nonlinearity.

TABLE I

LAW OF THE WALL CONSTANTS

	Re	A	B
This Study	7470	6.28 ± 2.5	5.19 ± 4.9
	12790	$5.66 \pm .70$	4.70 ± 1.45
Eckelmann & Reichardt	5600 & 8200	6.5	5.1
Patel & Head	6100	5.5	5.45

The velocity fluctuations nondimensionalized with the local mean velocity are shown in Figure 14. Both the corrected (Appendix B) and the uncorrected points are plotted. The corrected points tend to approach a limit of about .40 in the sublayer while the uncorrected points continue to increase.

The corrected velocity fluctuations were also normalized with the shear velocity and plotted against y^+ in Figure 15. The data compares well with both Hussain and Reynolds (1970) and with Eckelmann and Reichardt (1971).

Error Estimates

The 95% confidence intervals of the mean velocity measurements are summarized in Appendix C. These are based on a random error in the sampling and are generally less than 5%. Any systematic errors such as tape recorder speed or errors in the frequency to velocity conversion constant, are believed to be small, less than 1%.

The error in the estimates of the root-mean-square of the fluctuating velocity vary from 10% to 25% due to variations in the number of velocity samples.

CHAPTER IV

SUMMARY AND CONCLUSIONS

An individual realization dual scatter laser Doppler anemometer was successfully used to make measurements of both the mean and fluctuating velocities in the viscous sublayer of channel flow of water. Major problems caused by the turbulence and the small size of the region were overcome with special optical techniques. Two corrections were applied to the data, one for correcting the mean velocity due to turbulence, the other to correct the root-mean-square fluctuating velocity for the effect of the finite size of the probe volume in shear flow. The data are in good agreement with that of other researchers.

It can be concluded from this study that:

1) Use of the pedestal canceling optics substantially extended the velocity measuring range of the laser Doppler anemometer. The signals had less noise and with no electronic filter to set the near-wall measurements were made with confidence.
2) The probe volume miniaturization significantly improved the spatial resolution and allowed as many as four measurements to be made in the sublayer. The oval shape of the probe volume did not affect the measurements.
3) Measurements of the fluctuating velocity must take into account the effect of the finite size of the probe volume when the velocity gradient is large.

SELECTED BIBLIOGRAPHY

Bossel, H. H., W. J. Hiller, and G. E. A. Meier.

1972 "Noise Canceling Signal Difference Method for Optical Velocity Measurements." J. Physics, E., J. Sci. Instr. Vol. 5, 893.

Clark, J. A.

1968 "A Study of Incompressible Turbulent Boundary Layers in Channel Flow." Trans. ASME Series D. J. of Basic Engineering, 455-468.

Donohue, G. L., D. K. McLaughlin, and W. G. Tiederman.

1972 "Turbulence Measurements with a Laser Anemometer Measuring Individual Realizations." Phys. of Fluids, Vol. 15, 1920.

Durst, F., and J. H. Whitelaw.

1972 "Theoretical Considerations of Significance to the Design of Optical Anemometers." ASME Paper No. 72-HT-7, Presented at the Heat Transfer Conference, Denver, Colorado.

Eckelmann, H., and H. Reichardt.

1971 "Hot-Film Measurements in Oil." Proceedings of Symposium on Turbulence in Liquids.

Goethert, W. H.

1971 "Balanced Detection for the Dual Scatter LDV." AEDC-TR-71-70.

Hjelmfelt, A. T., and L. F. Mockros.

1965 "Motion of Discrete Particles in a Turbulent Field." Appl. Sci. Res., 16, 149.

Hussain, A. K. M. F., and W. C. Reynolds.

1970 "The Mechanics of a Perturabation Wave in Turbulent Shear Flow." Report FM-6, Department of Mechanical Engineering, Stanford, California: Stanford University.

McLaughlin, D. K., and W. G. Tiederman.

1973 "Biasing Correction for Individual Realization Laser Anemometer Measurementsin Turbulent Flows." Phys. of Fluids, Vol. 16, N12.

Patel, V. C., and M. R. Head.

1969 "Some Observations of Skin Friction and Velocity Profiles in Fully Developed Pipe and Channel Flows." J. Fluid Mech., Vol. 28, 181.

Reischman, M. M.

1973 "Laser Anemometer Measurements in Drag-Reducing Channel Flows." (Ph.D. dissertation, Oklahoma State University.)

Salsman, L. N., W. R. Advox, and D. K. McLaughlin.

1974 "An Evaluation of a Sequential Phase Comparison Data Processor for Laser Anemometry." Purdue Laser Doppler Anemometry Workshop.

Tiederman, W. G., D. K. McLaughlin, and M. M. Reischman.

1973 "Individual Realization Laser Doppler Technique Applied to Turbulent Channel Flow." Rolla, Missouri: Proceedings of the Symposium on Turbulence in Liquids.

APPENDIX A

STATISTICAL BIAS CORRECTION

APPENDIX A

STATISTICAL BIAS CORRECTION

One desired result from the ensemble of velocity realizations from a given location is an estimate of the time average velocity, $\overline{U_t}$, where

$$\overline{U}_t = \frac{1}{T} \int_t^{t+T} U(t)\, dt \qquad \text{(A-1)}$$

If the samples are independent, random and not biased by the experimental conditions this estimate is simply the ensemble average, $\overline{U}_e$.

$$\overline{U}_e = \frac{1}{N} \sum_{i=1}^{N} U_i \qquad \text{(A-2)}$$

Here N is the total number of individual velocity realizations, U_i. Unfortunately while the occurrence of an individual realization is a random event in time, the probability of a realization is dependent on flow conditions. This is because the seed is uniformly distributed throughout the water and hence the probability of obtaining a velocity realization is proportional to the volume of water flowing through the probe volume. Verification of this assumption about the seed distribution has been recently experimentally obtained by Salsman, Adcox and McLaughlin (1974). Consequently in high fluctuating flows

$$\overline{U}_e > \overline{U}_t \qquad \text{(A-3)}$$

because more fluid flows through the probe volume during the time the velocity is higher than $\overline{U}_t$ than it does during the time the velocity

is lower than $\overline{U}_t$. This yields more high velocity realizations than low velocity realizations.

McLaughlin and Tiederman (1973) have shown that $\overline{U}_e$ is substantially different from $\overline{U}_t$ when the root mean square of the fluctuations is greater than .05 of $\overline{U}_t$. However, a properly weighted ensemble average,

$$\overline{U} = \frac{\sum_{i=1}^{N} \omega_i U_i}{\sum_{i=1}^{N} \omega_i} \qquad \text{(A-4)}$$

will yield a good estimate of $\overline{U}_t$. The proper weighting function is inversely proportional to the volume of fluid swept through the probe volume. Hence ω_i depends upon the magnitude of the instantaneous velocity vector as well as a geometric function which gives the orientation of the vector with respect to the probe volume. In this experiment neither of these are known. However, using models of turbulent flow, McLaughlin and Tiederman (1973) have shown that the reciprocal of the streamwise velocity component is a good approximation to the true weighting functions. Consequently, Equation 3 becomes

$$\overline{U} = \frac{\sum_{i=1}^{N} \left(\frac{1}{U_i}\right) U_i}{\sum_{i=1}^{N} \frac{1}{U_i}} \qquad \text{(A-5)}$$

or

$$\overline{U} = \frac{N}{\sum_{i=1}^{N} \frac{1}{U_i}} \qquad \text{(A-6)}$$

and

$$\overline{U} \approx U_t \qquad \text{(A-7)}$$

It should be noted that $\overline{U}$ is inversely proportional to the ensemble average of the individual Doppler periods and hence the calculation is quite straight forward.

APPENDIX B

EFFECTS OF A FINITE SIZED PROBE VOLUME IN SHEAR FLOW

APPENDIX B

EFFECTS OF A FINITE SIZED PROBE VOLUME IN SHEAR FLOW

A simple mathematical model of the flow field of the viscous sublayer is postulated in this appendix and used to predict the effect of the size of the probe volume on the mean velocity and root-mean-square of the velocity fluctuation measurements.

Flow Model

Since the largest velocity gradient in channel flow occurs near the wall, a correction for the finite size of the probe volume is needed most in the viscous sublayer. The following model and correction is derived for only this region. In the viscous sublayer the mean velocity profile is linear with distance from the wall and the velocity fluctuations are a linear function of distance from the wall. That is to say the fluctuations are constant percentage of the mean velocity at any point in the flow. The velocity fluctuations were modeled by a sine wave. The flow field is then described by

$$U(y,t) = sy + (ksy)(\sin t) \qquad \text{(B-1)}$$

where U is the velocity, s is the velocity gradient, y is the distance from the wall, k is a constant relating the velocity fluctuation to the mean and t is time. The probe volume placed in the flow field has a width of w and its center is a distance 1 away from the wall. In this

analysis it will be assumed that all particles that pass through ten fringes inside the $\frac{1}{e^2}$ contour will be the only particles detected, and that signal amplitude has no effect on the measurement. The only bias in the ensemble of velocity measurements is due to greater probability of a realization at a high velocity than at a low velocity. It will also be assumed that the particle does not change velocity while in the probe volume.

Effect on the Mean Velocity Measurement

The desired quantity is the time average velocity through the probe volume, or

$$U_t = \frac{1}{Tw} \iint U(y,t)dtdy \qquad \text{(B-2)}$$

For the flow field described by Equation B-1 and integrating over the probe volume and one cycle of turbulence this becomes

$$U_t = sl \qquad \text{(B-3)}$$

The time average velocity, $\overline{U}_t$, is the velocity at the center of the probe volume, sl.

As show by McLaughlin and Tiederman (1973) and summarized in Appendix A, the time average velocity can be estimated from individual realization laser Doppler anemometry data by correcting the statistical bias with this one dimensional correction:

$$U = \frac{\sum_{i=1}^{N} \frac{1}{U_i} U_i}{\sum_{i=1}^{N} \frac{1}{U_i}} = \frac{N}{\sum_{i=1}^{N} \frac{1}{U_i}} \qquad \text{(B-4)}$$

If the only bias in the velocity realization ensemble is due to the greater probability of realizations at a high velocity, then, Equation B-4 estimates the time-average velocity for the entire volume flow through the probe volume. Equation B-4 corrects the bias caused by velocity fluctuation from the turbulence and the velocity gradient. Moreover when the velocity gradient is linear, the time-average velocity at the center of the probe volume is the same as the time-average velocity for the entire volume flow. Consequently when the gradient is linear, the estimate from Equation B-4 is the correct estimate of the time-average velocity at the geometric center of the probe volume.

The Effects on the Root-Mean-Square Velocity Fluctuations

The root-mean-square velocity fluctuation is defined by

$$\overline{u'^2} = \frac{1}{Tw} \iint (U(t,y) - U_m)^2 dt dy \qquad \text{(B-5)}$$

For the flow field described by Equation B-1 and using $U_m = s1$, Equation B-5 can be integrated of the probe volume and time resulting in

$$\overline{u'^2} = \frac{s^2w^2}{12} + \frac{s^2k^2l^2}{2} + \frac{s^2k^2w^2}{24} \qquad \text{(B-6)}$$

The velocity fluctuations in the probe volume are a combination of three effects, $s^2w^2/12$, the change in mean velocity across the probe volume, $s^2k^2l^2/2$, the velocity fluctuations due to turbulence at the mean and $s^2k^2w^2/24$, the change in velocity fluctuations across the probe volume.

The velocity fluctuation in the probe volume can be estimated from individual realization laser Doppler anemometry data and an equation derived by McLaughlin and Tiederman (1973):

$$\overline{u'^2} = \frac{\sum_{i=1}^{N} \frac{1}{U_i} \left(U_i - U_m\right)^2}{\sum_{i=1}^{N} \frac{1}{U_i}} \qquad \text{(B-7)}$$

This estimates the fluctuation throughout the entire probe volume. The usual desired quantity is the root-mean-square fluctuations at the centerline. Since s, w, l, and $\overline{u'^2}$ are all known, Equation B-6 can be solved for k. The velocity fluctuations at the centerline or mean velocity can be calculated by evaluating $s^2k^2l^2/2$.

The error in using Equation B-7 to estimate the root-mean-square velocity fluctuations is significant only when the change in mean velocity across the probe volume is of the same order of magnitude as the root-mean-square of the velocity fluctuations. In channel flow this occurs in the near wall region.

APPENDIX C

DATA

Re = 7470 Data Run 3 U = .0633 ft/sec

y	y^+	N	$\bar{U}_{EA}$	$\bar{U}_{TA}$	u^+	% Error	u'	u'_c	$\frac{u'}{U}$
.00355	1.462	286	.1094	.0929	1.468	5.7	.0459	.0413	.446
.00551	2.288	260	.1674	.1480	2.339	5.0	.0613	.0582	.393
.00942	3.974	260	.2821	.2504	3.957	4.6	.0965	.0945	.378
.01333	5.669	260	.4015	.3563	5.631	3.7	.1394		.391
.02114	9.138	260	.5837	.5355	8.462	3.7	.1645		.307
.0310	13.62	195	.7255	.6802	10.75	3.55	.1721		.253
.0466	20.65	169	.8426	.8098	12.79	3.0	.1611		.199
.0700	31.28	143	.9321	.9033	14.27	2.7	.1500		.166
.1208	54.45	117	1.0135	.9974	15.72	2.2	.1217		.122
.2487	113.05	104	1.1739	1.1674	18.448	1.45	.0877		.075
.4987	228.67	104	1.2606	1.258	19.88	.87	.0569		.045

Re = 12,790 Data Run 4 U = .0968 ft/sec

y	y^+	N	U_{EA}	U_{TA}	u^+	% Error	u'	$\frac{u'}{c}$	$\frac{u'}{U}$
.00214	1.569	286	.1835	.1550	1.6016	4.9	.0789	.0595	.3859
.00410	3.005	260	.3324	.2902	2.9986	4.7	.1285	.1172	.404
.00605	4.518	260	.4979	.4334	4.4781	4.4	.1819	.1764	.407
.00996	7.578	221	.7169	.6212	6.4186	4.2	.2296		0.370
.01386	10.545	195	.8327	.7648	7.9024	3.9	.2352		0.307
.01777	12.649	208	1.0000	.9268	9.5764	3.4	.2523		0.272
.02167	16.645	195	1.0996	1.0294	10.6364	3.2	.2580		0.251
.03144	24.381	146	1.1757	1.1075	11.4434	3.5	.2554		0.231
.04706	36.494	130	1.3650	1.3332	13.7755	2.4	.1971		0.148
.07050	55.202	104	1.4177	1.3948	14.4121	2.4	.1775		0.127
.12130	95.910	104	1.5366	1.5201	15.7067	1.9	.1553		0.102
.2492	197.038	104	1.7307	1.7221	17.7939	1.32	.1191		0.069
.4992	394.711	65	1.8856	1.8856	1.8824	1.	.0776		0.041

APPENDIX D

FIGURES

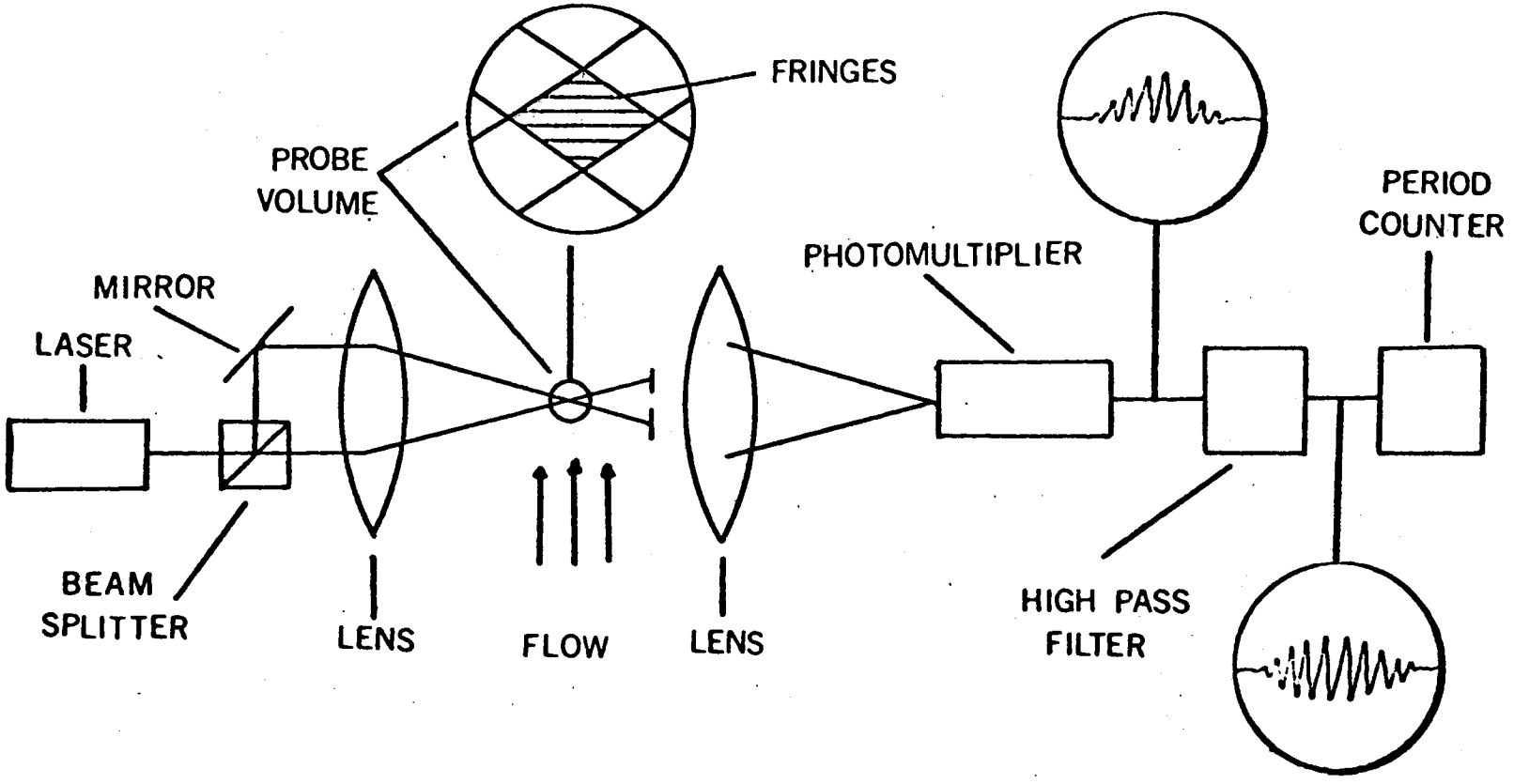

Figure 1. A Basic Dual Scatter Laser Doppler Anemometer

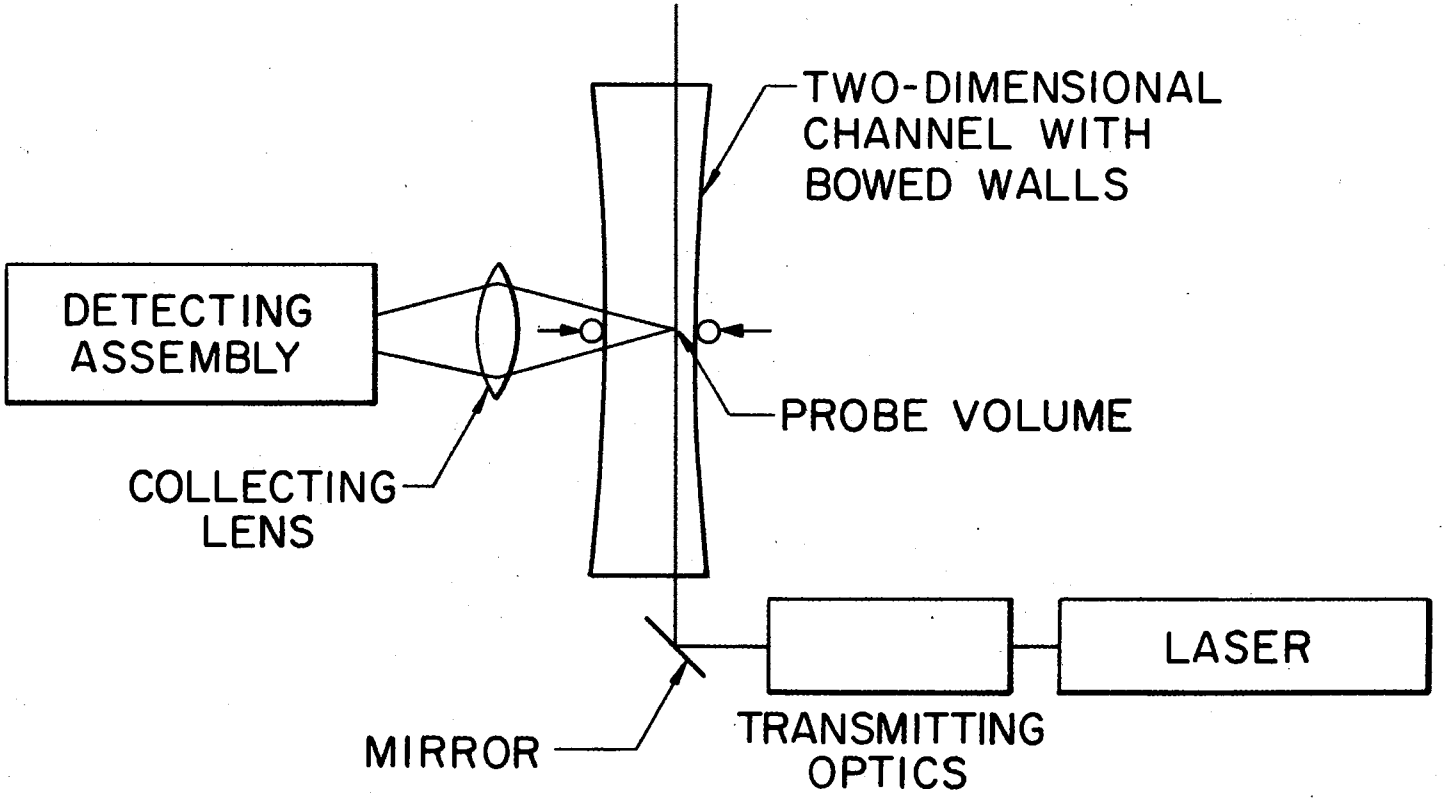

Figure 2. Schematic of Flow Channel and the Anemometer

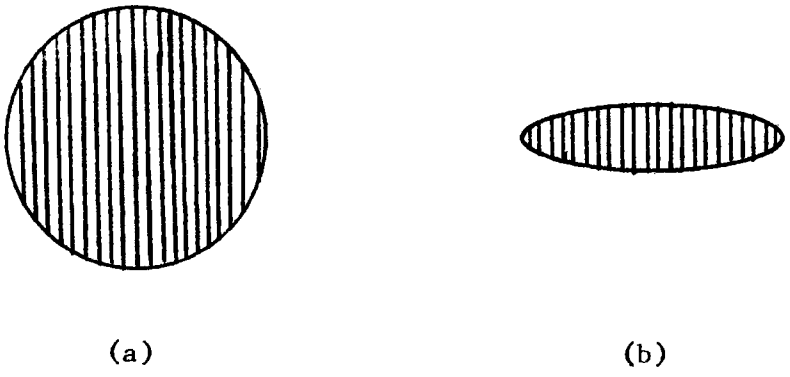

Figure 3. Probe volume shape. (a) Normal probe volume, (b) Probe volume shrunk in y-dimension

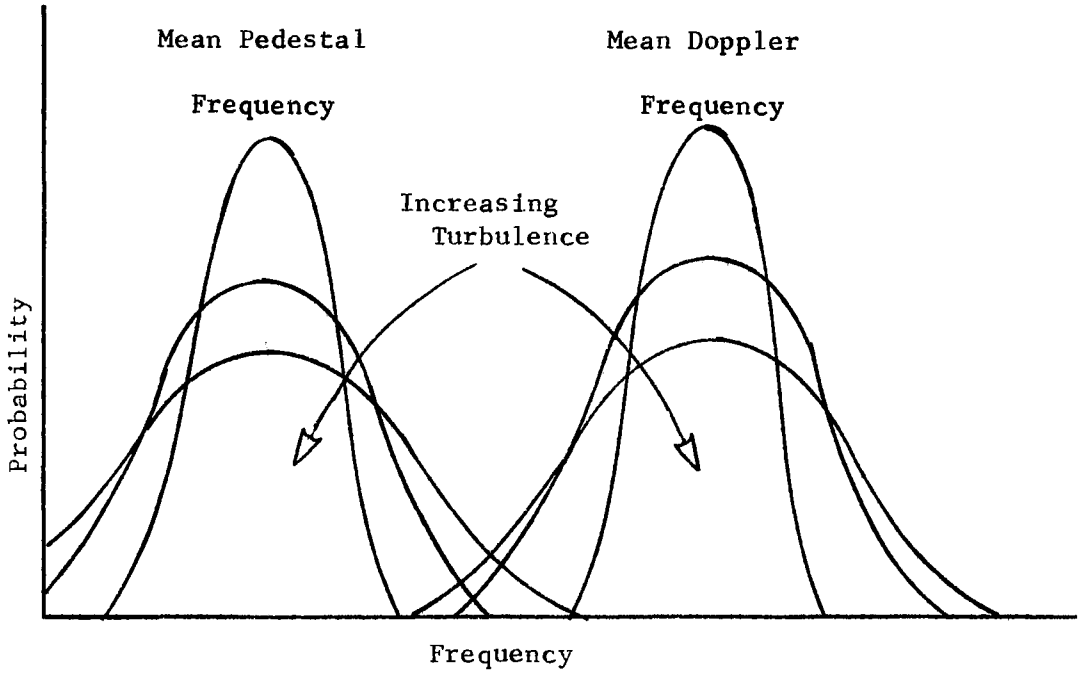

Figure 4. Histograms of Doppler and Pedestal Frequency

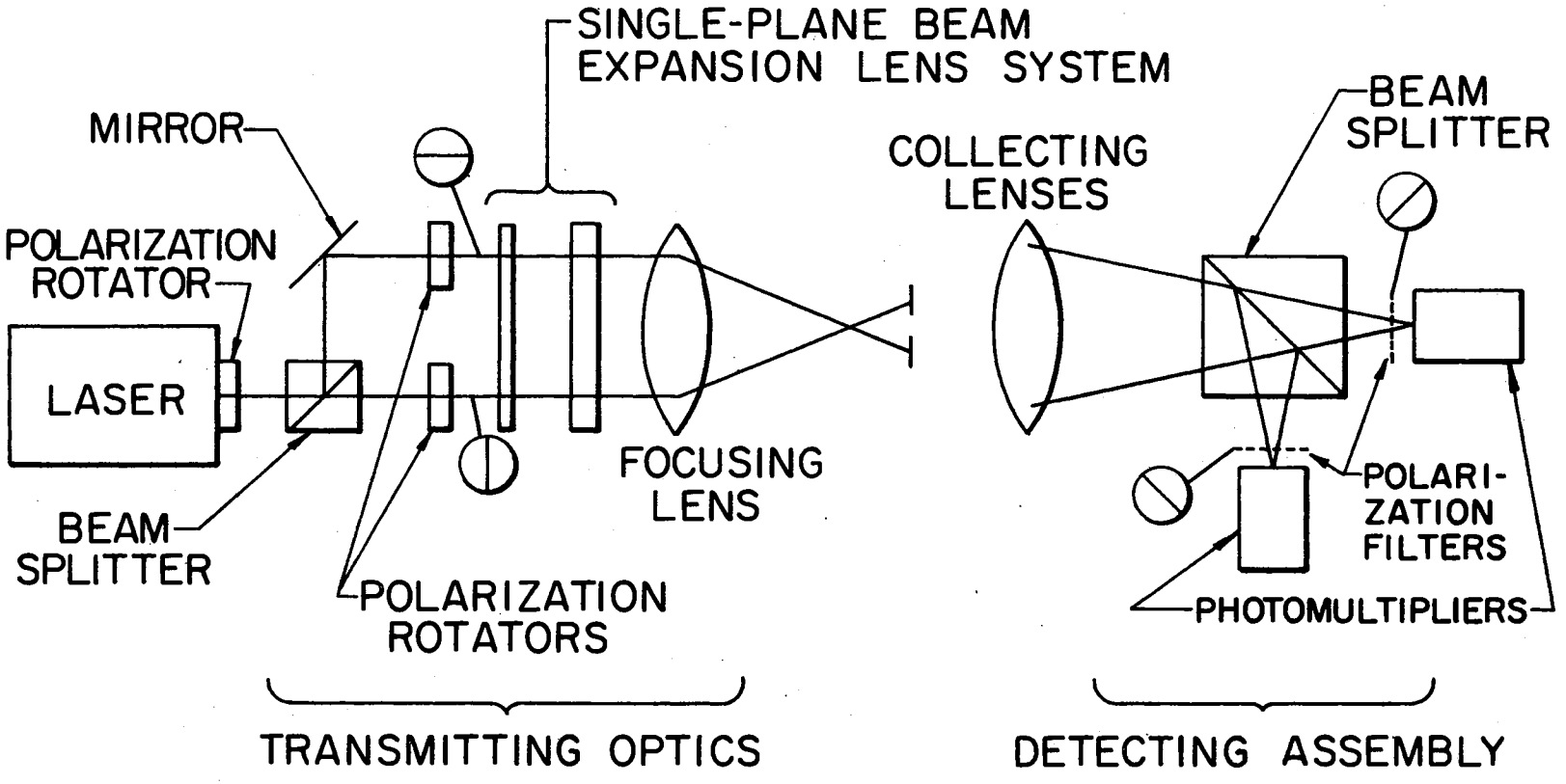

Figure 5. Schematic of the Optical System

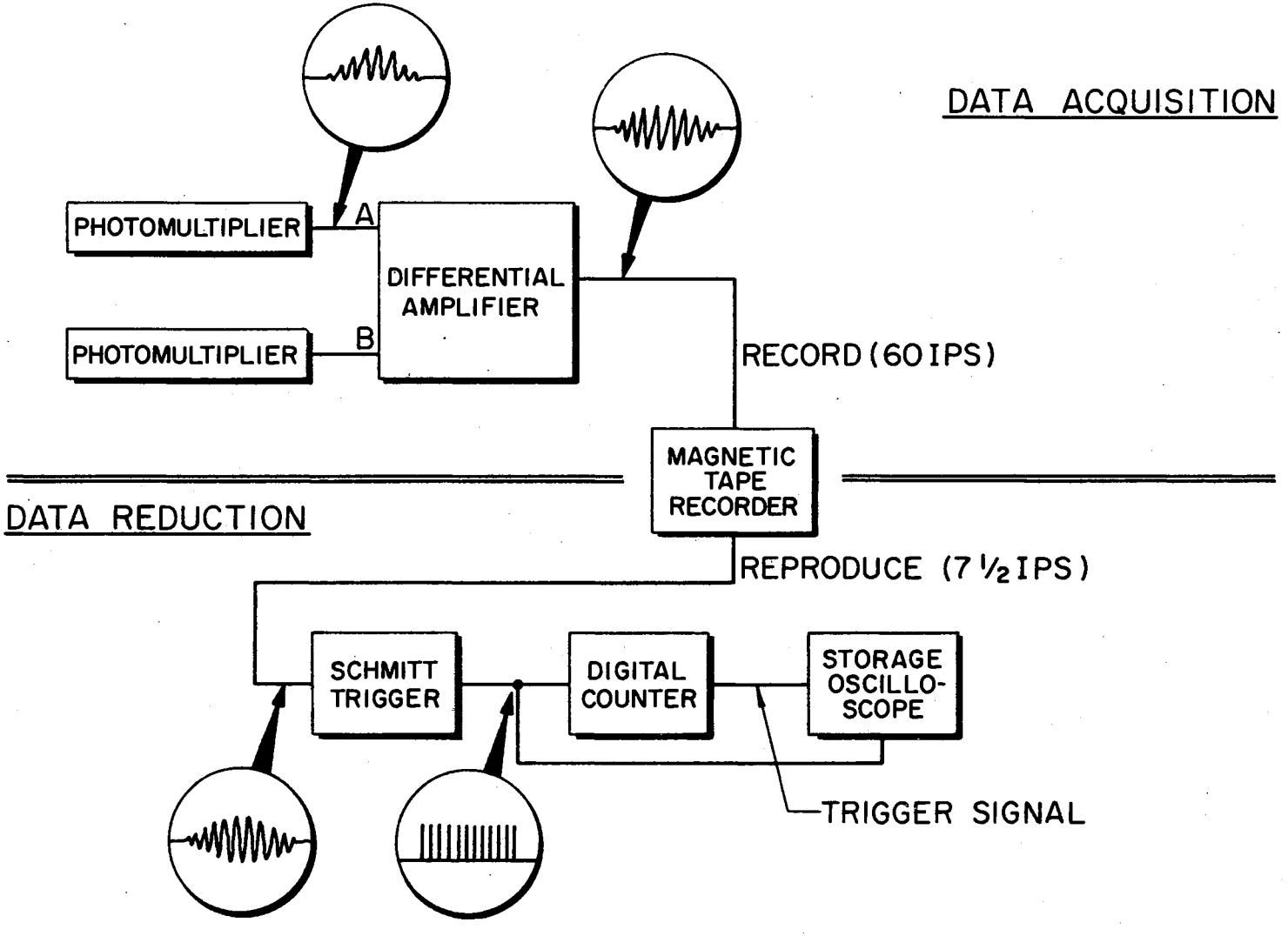

Figure 6. Block Diagram of the Data Acquisition Electronics

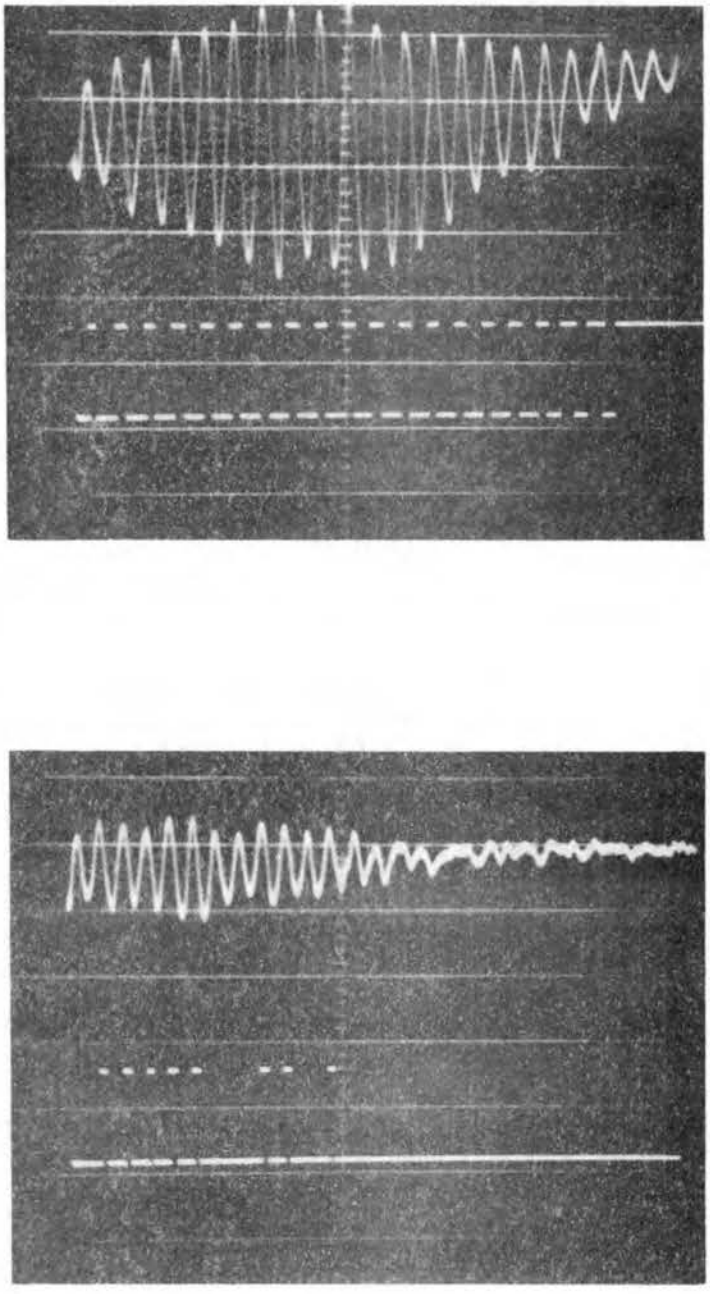

Figure 7. (a) Good Pulse Train. (b) Pulse Train with dropped pulses.

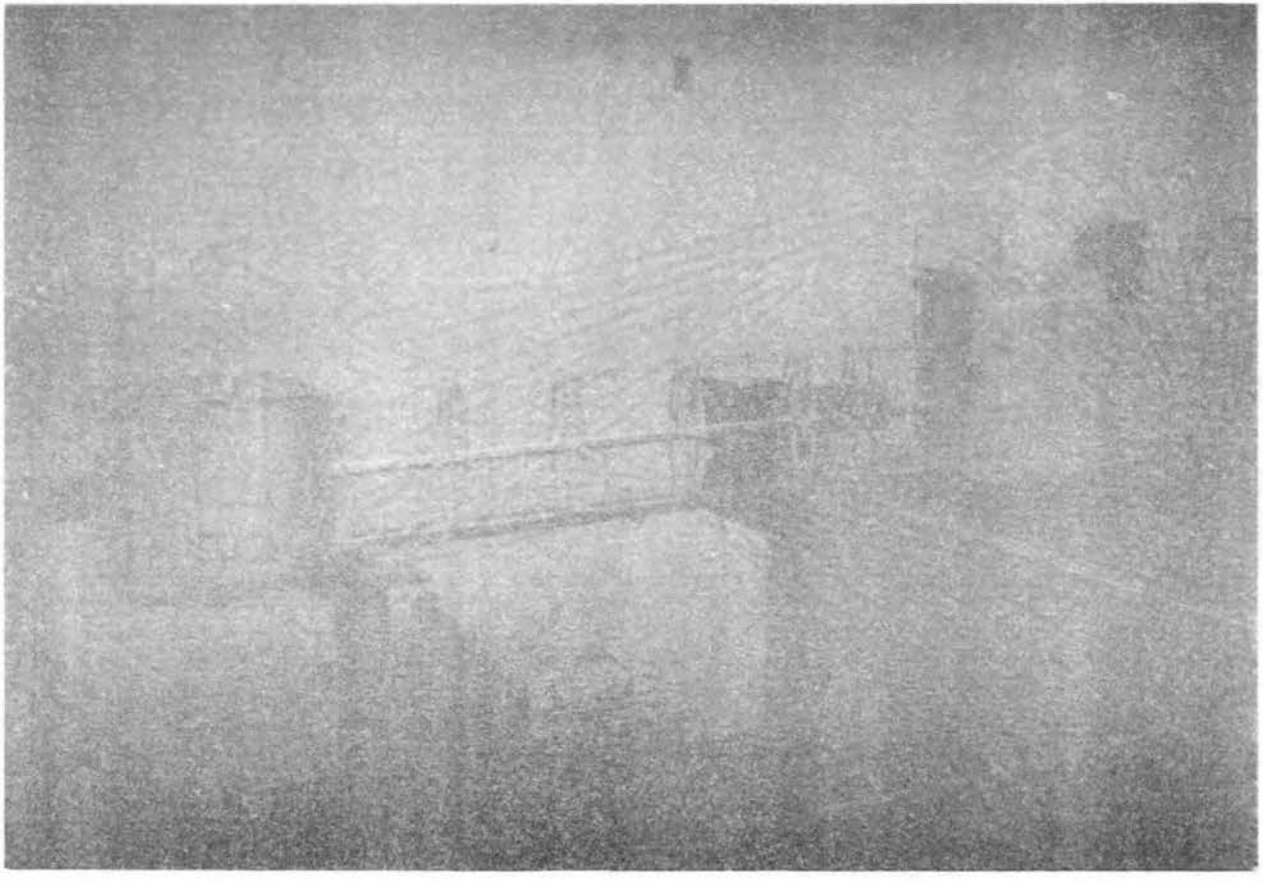

Figure 8. Photograph of Flow Channel and Anemometer

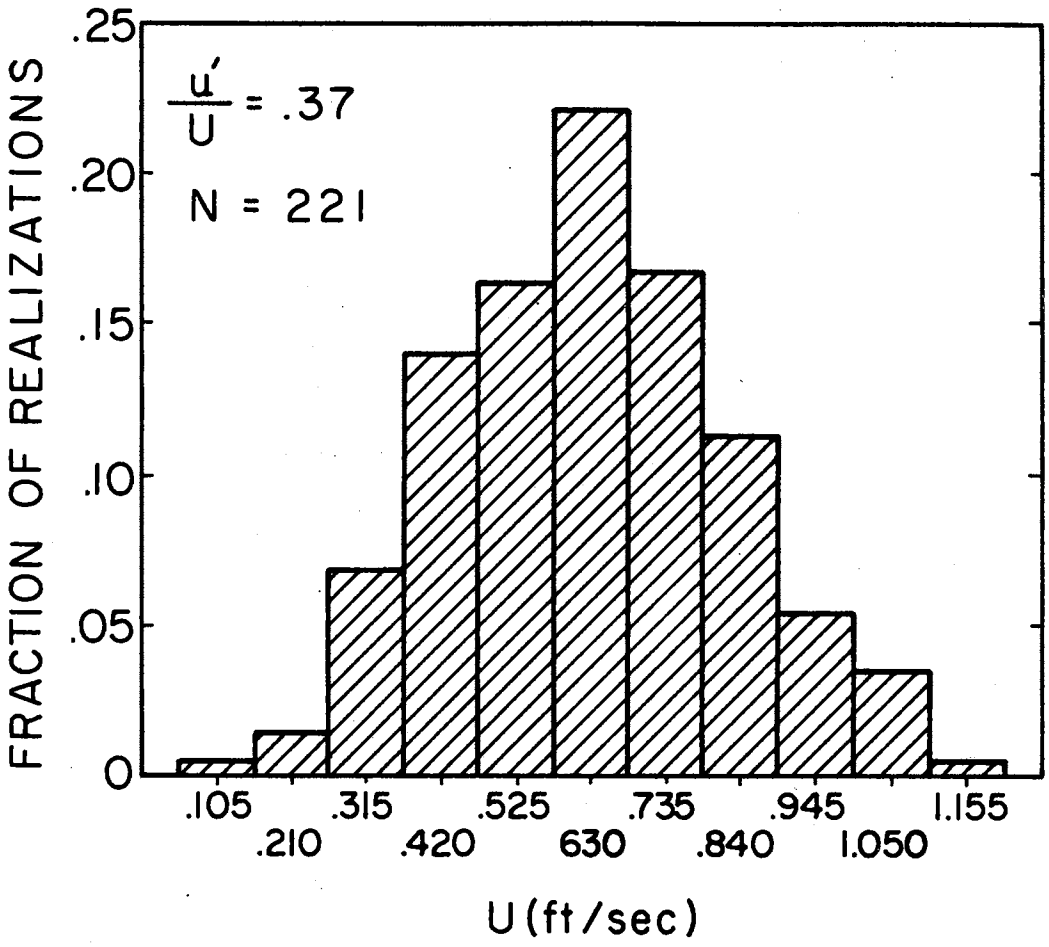

Figure 9. Histogram of Velocity Realizations in Turbulent Channel Flow, Re=12,790, y^+=7.5.

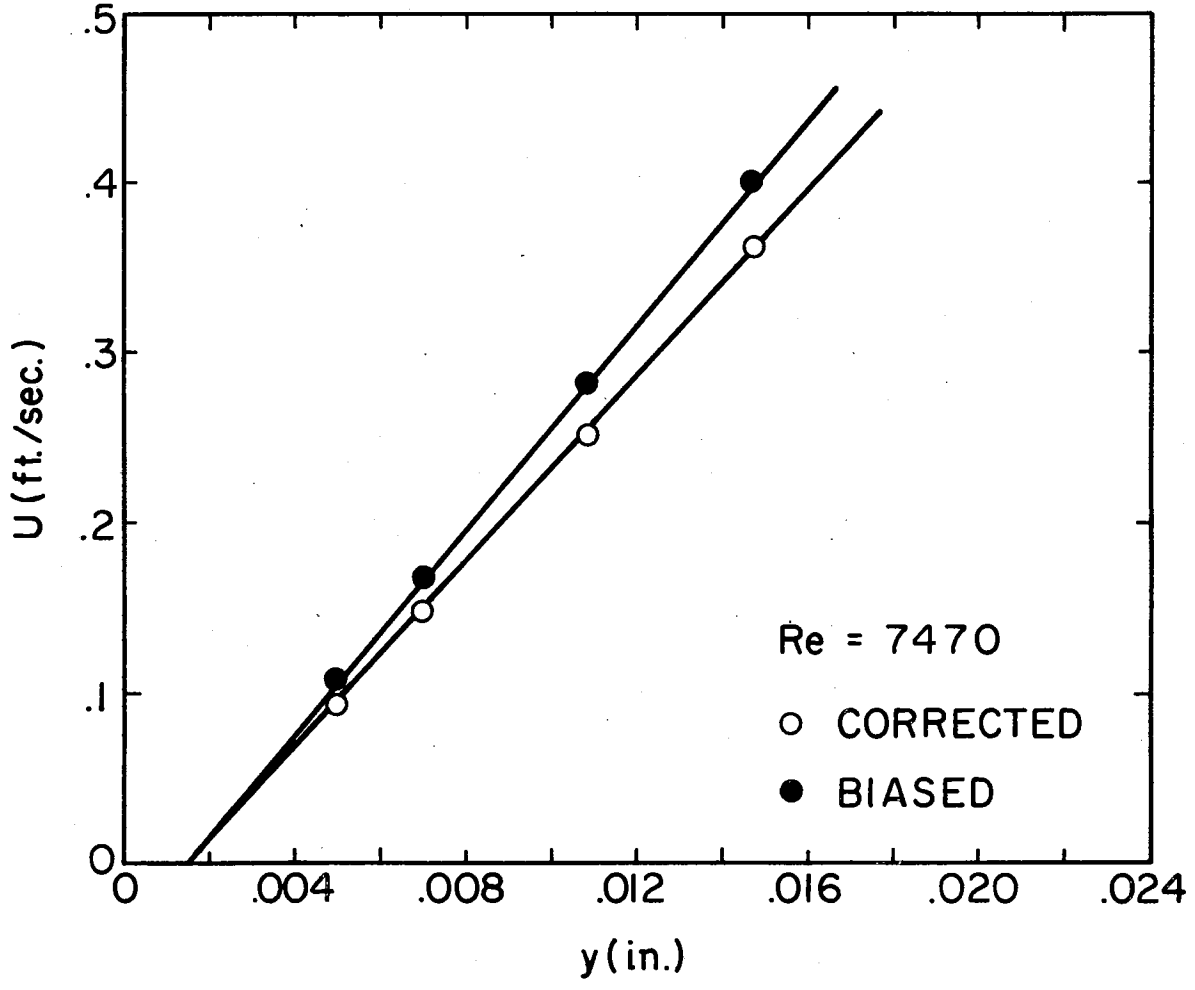

Figure 10. Mean Velocity Profile in Viscous Sublayer

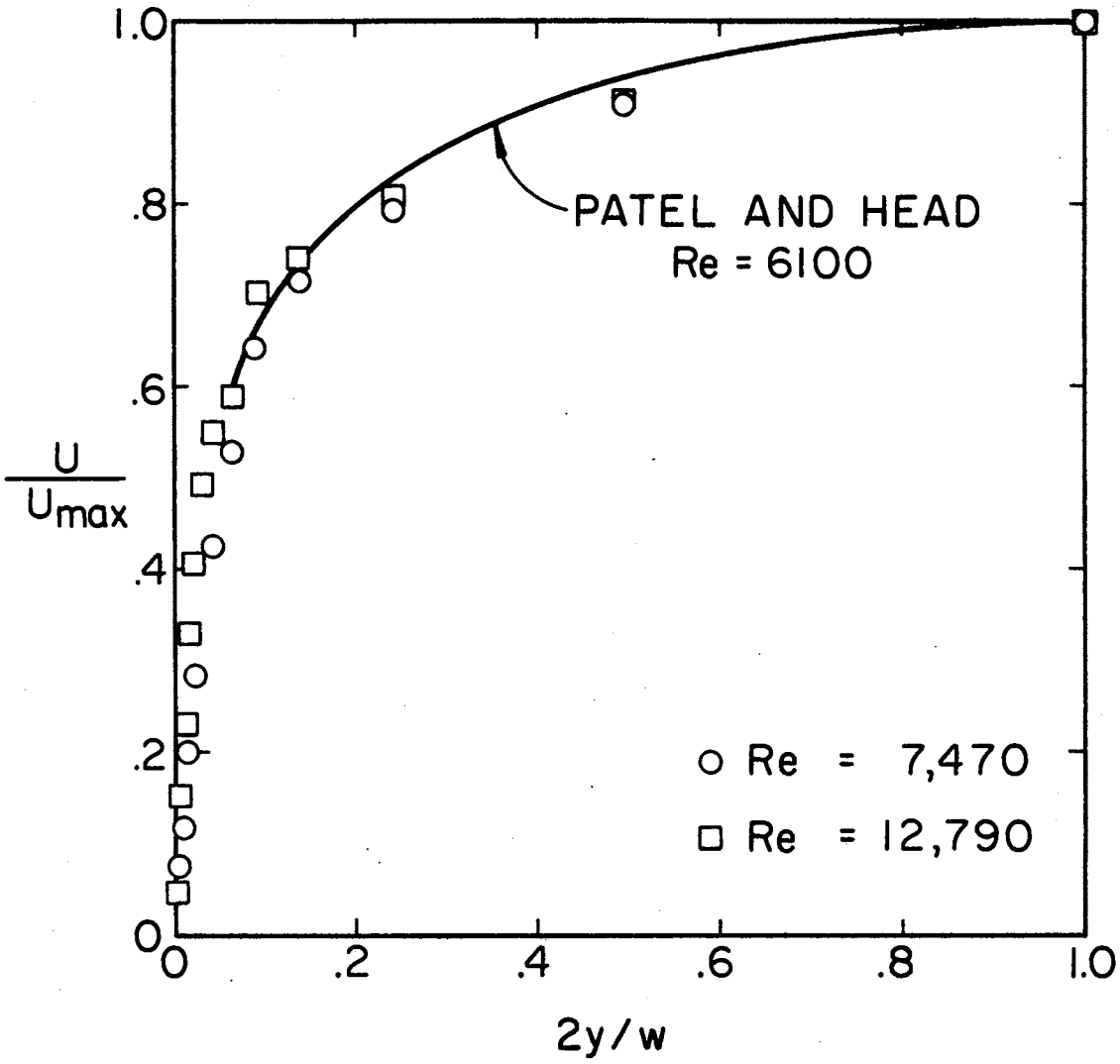

Figure 11. Non-dimensional Mean Velocity Profiles

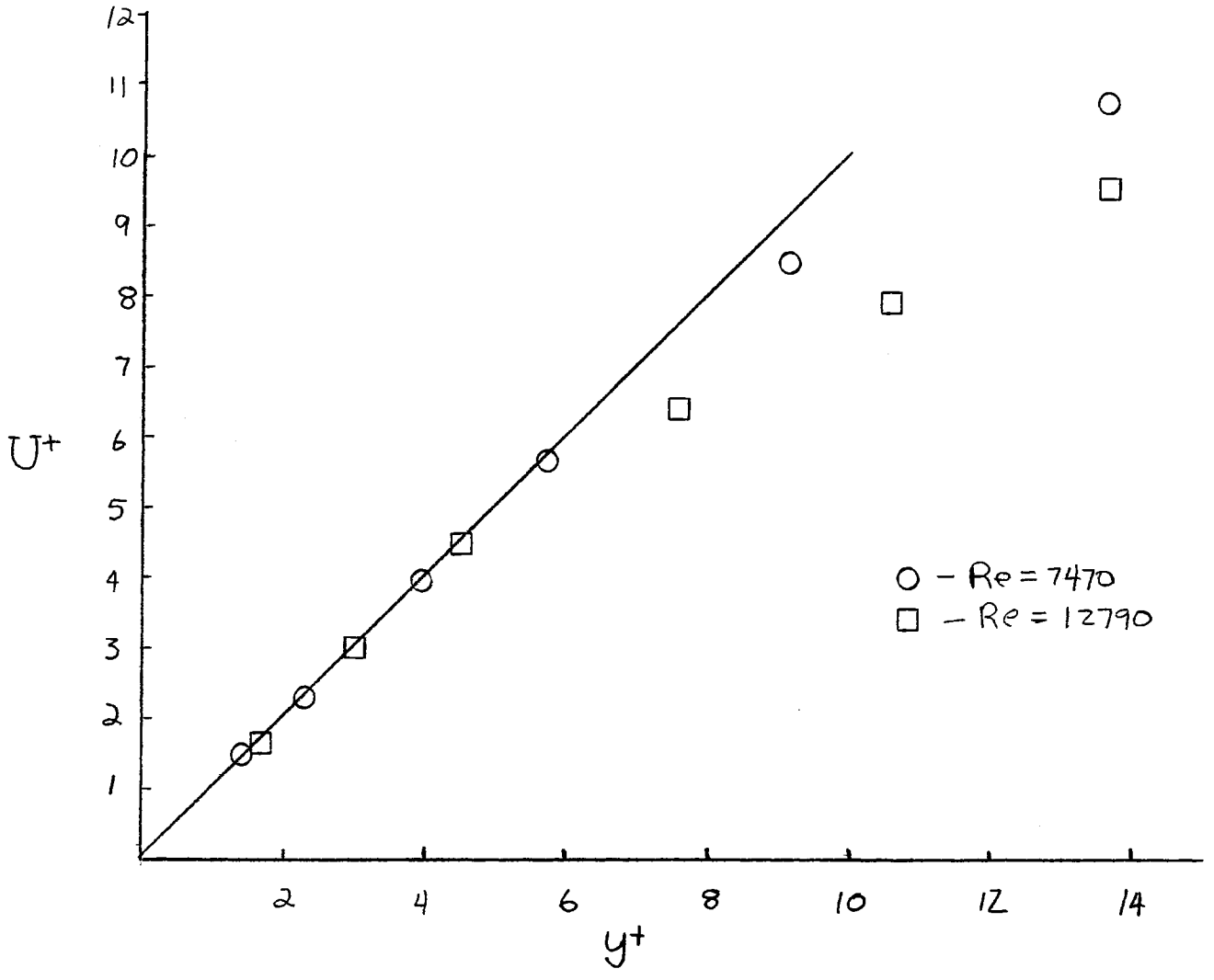

Figure 12. Near Wall Profile in Law of the Wall Coordinates

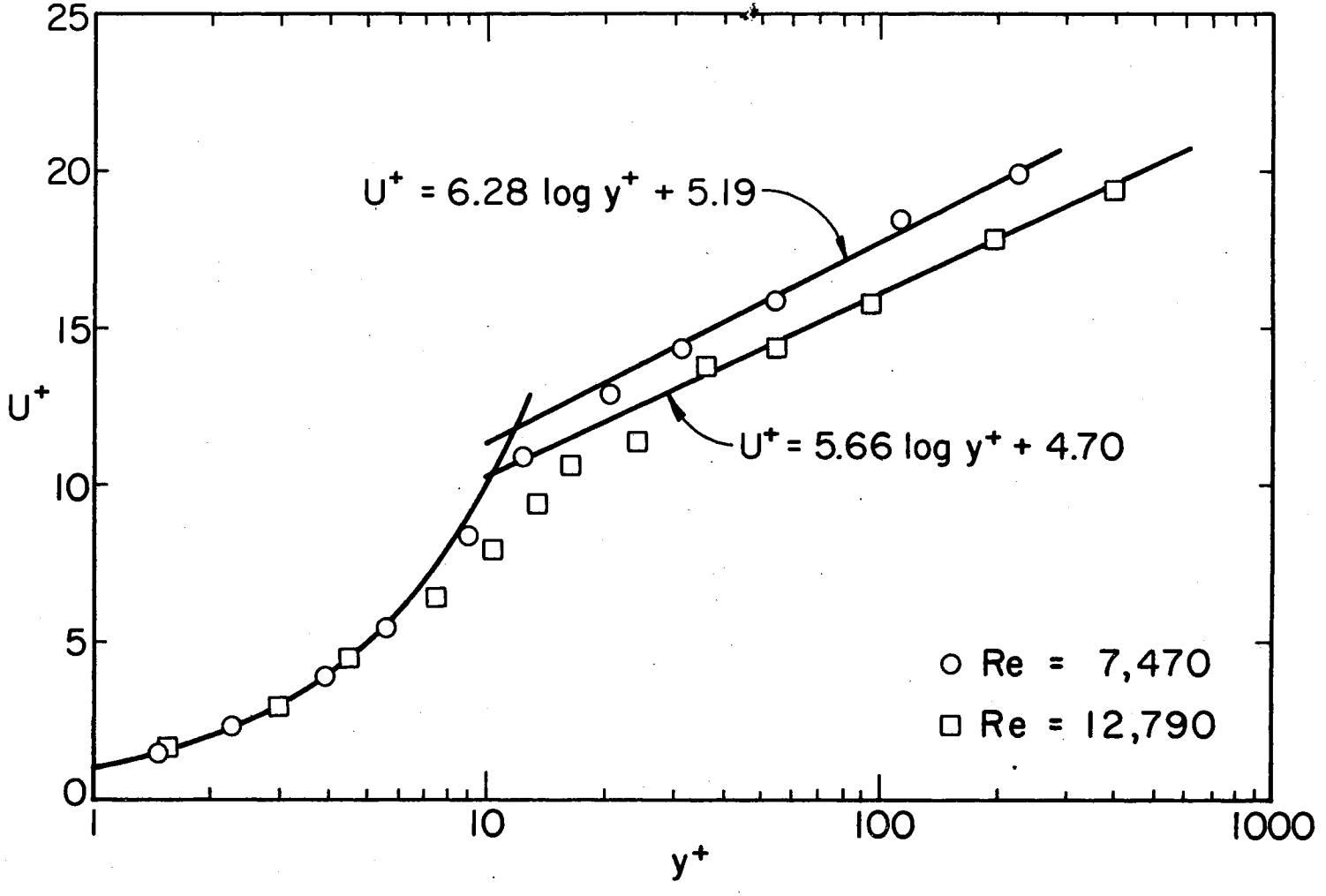

Figure 13. Mean Velocity Profiles in Law-of-the-Wall Coordinates

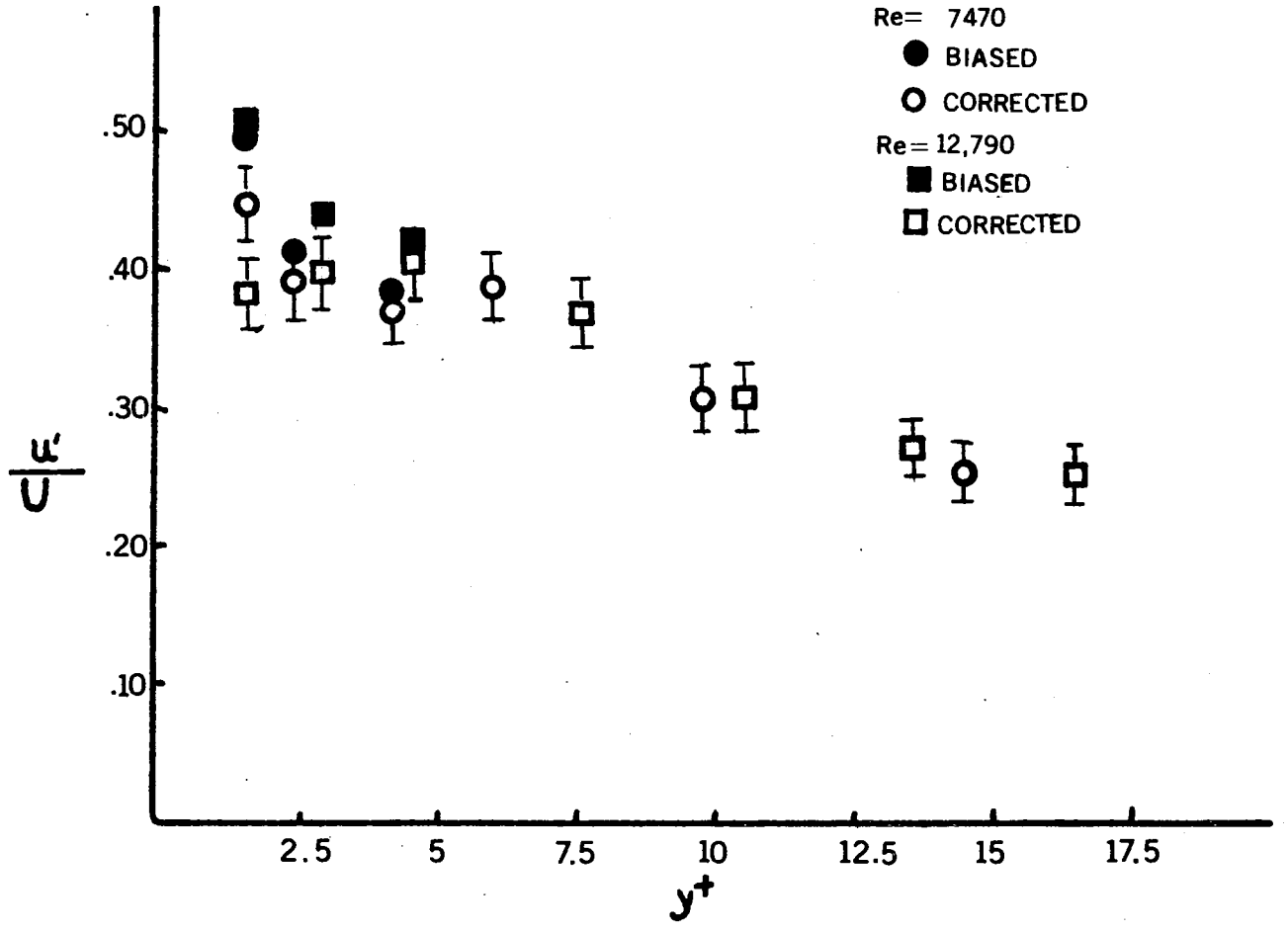

Figure 14. Streamwise Turbulent Intensity

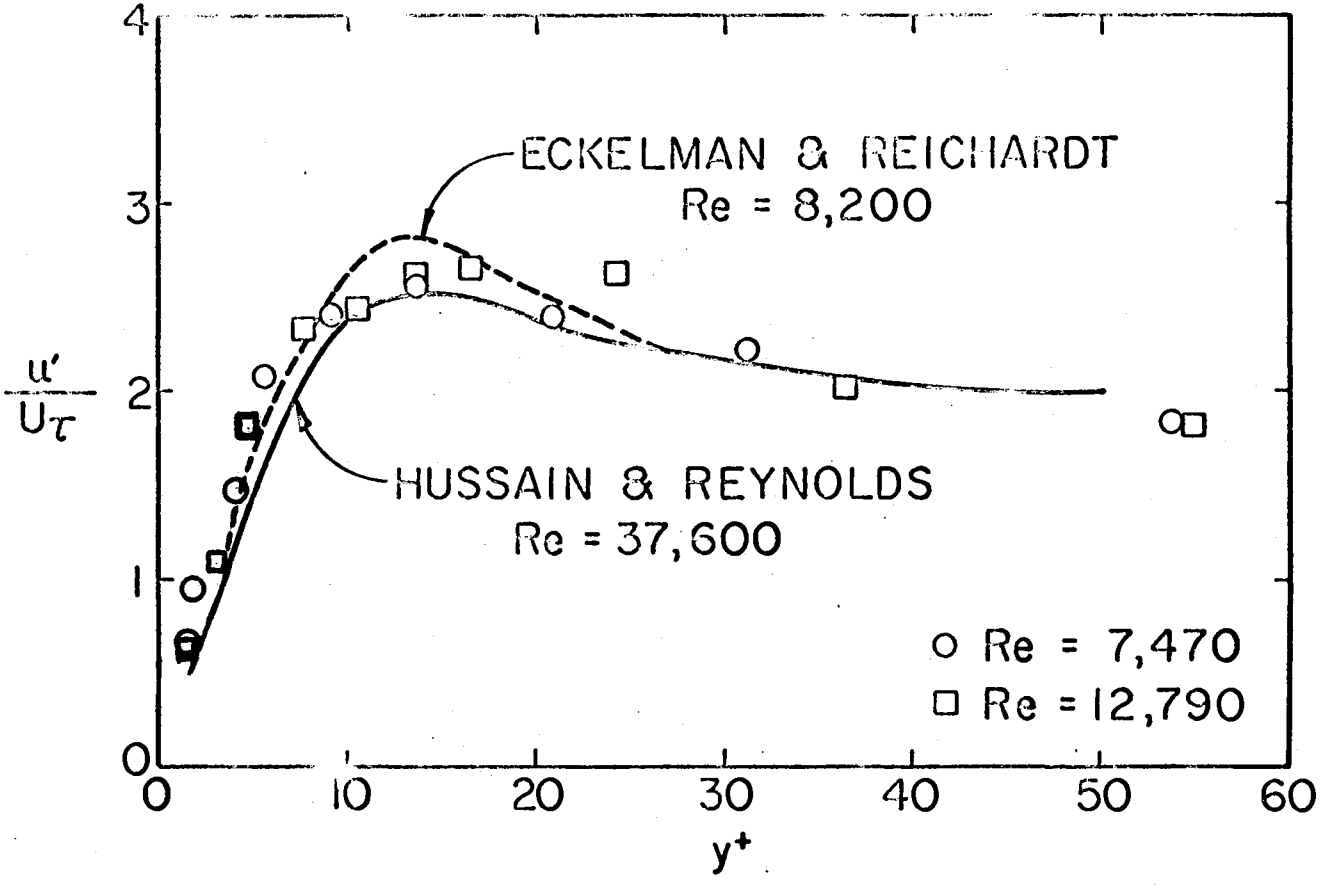

Figure 15. Streamwise Turbulence Intensity Profiles

VITA

Michael E. Karpuk

Candidate for the Degree of

Master of Science

Thesis: A LASER DOPPLER ANEMOMETER FOR VISCOUS SUBLAYER MEASUREMENTS

Major Field: Mechanical Engineering

Biographical:

Personal Data: Born in Sioux City, Iowa, November 11, 1949, the son of Mr. and Mrs. Edward J. Karpuk.

Education: Graduated from McLain High School, Tulsa, Oklahoma, in May, 1967; received Bachelor of Science degree in Mechanical Engineering from Oklahoma State University in May, 1972; completed requirements for Master of Science degree at Oklahoma State University in May, 1974.

Professional Experience: Graduate assistant, Oklahoma State University, 1972-73; research assistant, School of Mechanical and Aerospace Engineering, Oklahoma State University, 1973-74.

Professional Organizations: National Society of Professional Engineers and AIAA.